J Solid State Electrochem (1998) 2: 413–419

ORIGINAL PAPER

Dirk A. Fiedler · Jörg H. Albering · Jürgen O. Besenhard

Characterization of strontium and barium manganates by abrasive stripping voltammetry

Received: 25 November 1997 / Accepted: 28 January 1998

Abstract Abrasive stripping voltammetry is applied in order to characterize barium and strontium manganates-(V) and -(VI) in solid state phases. Voltammetric reduction peak potential values of $KBaMnO_4$, $Ba_3(MnO_4)_2$, $Ba_3(MnO_4)_{2-x}(BO_3)_x$ ($x = 0.031(1)$), $Ba_5(MnO_4)_3OH$, $Ba_5(MnO_4)_3Cl$, $Sr_5(MnO_4)_3OH$ and $BaMnO_4$ are shown to be proportional to the corresponding average Mn-O distances, which were determined from X-ray powder diffractometric data through Rietveld refinement analyses.

Key words Abrasive stripping voltammetry · X-ray powder diffractometry · Manganates · Solid state electrochemistry

Introduction

The recently introduced electroanalytical technique of abrasive stripping voltammetry [1–4] has been used in order to characterize solid compounds irrespective of their conductive properties [5–8]. The analytical time scale may be dramatically reduced when analyzing poorly conductive manganese dioxides and spinel-type manganates by using this technique [9]. Evidence of manganates-(V) has existed since the early work of Rosenstiehl [10]. However, the presence of manganese in its formally pentavalent state was recognized some 100 years later by Lux [11]. Since then, a number of manganates-(V) have been prepared and characterized [12–14]. In this contribution, we focus on the voltammetric analysis of solid manganates (V) and (VI) and the correlation with X-ray powder diffractometric data [15].

D.A. Fiedler · J.H. Albering (✉) · J.O. Besenhard
Institut für chemische Technologie anorganischer Stoffe,
Technische Universität Graz, Stremayrgasse 16/III,
A-8010 Graz, Austria
Tel.: +43-316-873 8763, Fax: +43-316-873 8272,
e-mail: f537albe@mbox.tu-graz.ac.at

Experimental

Preparation

All chemicals were of at least analytical grade, and purchased from either Aldrich, Merck, Riedel-de Haën or Fluka chemical companies (Germany). All products were characterized by powder X-ray diffractometry as described below. Except for the manganates-(V) $Ba_3(MnO_4)_{2-x}(BO_3)_x$ ($x = 0.031(1)$) and $Ba_5(MnO_4)_3Cl$, corresponding lattice constants were reported earlier [15].

$KBaMnO_4$ was prepared from $KMnO_4$ and $Ba(OH)_2 \cdot 8H_2O$ in a KOH/H_2O melt at 350–400 °C, pouring the hot reaction mixture in 1 M KOH and filtering off the product.

Low-temperature (LT) $Ba_3(MnO_4)_2$ was precipitated by reducing $BaMnO_4$ with ethanol in a boiling solution of $Ba(OH)_2 \cdot 8\ H_2O$ in analogy to the procedure described by Scholder and Klemm [12, 13].

High-temperature (HT) $Ba_3(MnO_4)_2$ was prepared by solid-state reaction of MnO_2 in a $Ba(NO_3)_2$ flux at 650 °C, dissolving the cold reaction mixture in water and filtering off the product. Similarly, $Ba_3(MnO_4)_{2-x}(BO_3)_x$ ($x = 0.031(1)$) was the product when starting with a mixture of MnO_2 and H_3BO_3 in a $Ba(NO_3)_2$ flux at 650 °C. The boron content was determined after dissolution of the compound in HCl by the inductively coupled plasma technique at the Institute of Analytical Chemistry of Graz University of Technology.

$BaMnO_4$ was precipitated from $KMnO_4$ and $Ba(OH)_2 \cdot 8H_2O$ in boiling 3 M KOH [12, 13]. $Ba_5(MnO_4)_3OH$ was obtained by reduction of $KMnO_4$ with ethanol in a solution of $Ba(OH)_2 \cdot 8H_2O$ and 1 M KOH.

Single-phase $Ba_5(MnO_4)_3Cl$ could not be isolated as a product from the high-temperature flux reaction described earlier [14]. However, when simply heating a stoichiometric mixture of $Ba_3(MnO_4)_2$ and $BaCl_2$ to 750 °C, the pure product was obtained as a dark green powder.

$Sr_5(MnO_4)_3OH$ was synthesized by reacting $KMnO_4$ and $Sr(NO_3)_2 \cdot xH_2O$ in a KOH/H_2O melt at 400 °C, pouring the hot reaction mixture into 1 M KOH and filtering off the product.

X-ray powder diffraction

X-ray powder diffraction (XPD) patterns were collected with either an automated Siemens D500 diffractometer with Bragg-Brentano geometry combined with a scintillation counter or a Stoe STADI/P focussing monochromatic beam diffractometer with a rotating sample in the symmetric transmission mode and a linear position sensitive detector. Cu Kα radiation (Cu Kα_1 in case of the STADI/

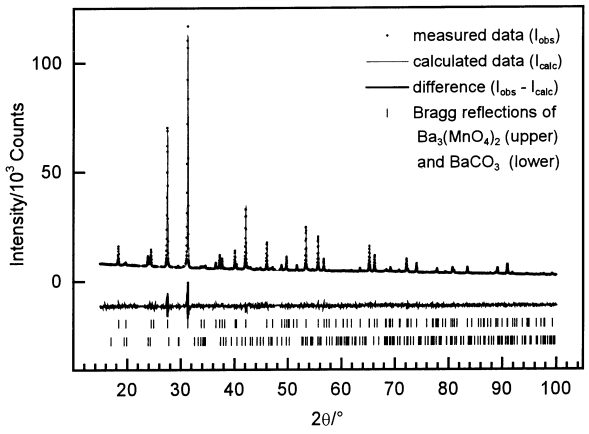

Fig. 1 X-ray powder diffractogram of HT-$Ba_3(MnO_4)_2$ (Stoe STADI/P diffractometer) recorded in the symmetric transmission mode at a step width of 0.02° (2θ scale) and a counting time of 10 s per step

P diffractometer) was used for the measurements. A constant step width of 0.02° (2θ scale) and counting times varying between 10–120 s per step were applied.

Rietveld structure refinements

The XPD patterns were analyzed by Rietveld least-squares structure refinements with the aid of the RIETAN [16] program. The unit cell, atomic positional, isotropic thermal, Pseudo-Voigt line profile, polynomial background and zero-point correction parameters were refined independently in subsequent least-squares cycles. The peak asymmetry (especially for data from reflection mode measurements in the absence of automatic divergence slits) was included in the refinements in the 2θ range lower than 50°. The X-ray powder diffractogram of the high-temperature phase HT-$Ba_3(MnO_4)_2$ is shown, as an example, in Fig. 1. Lattice constants of the alkaline earth manganates-(V) and -(VI) as calculated from Rietveld refinement analyses as well as average Mn-O distances are collected in Table 1. More detailed information regarding the crystallographic systems and approximate crystal dimensions are shown in Table 2. Clearly, low-temperature preparation methods lead to lower crystallinity and strong intergrowth of crystals ($KBaMnO_4$, LT-$Ba_3(MnO_4)_2$, $Ba_5(MnO_4)_3OH$ and $BaMnO_4$), while high-temperature syntheses generate highly crystalline manganates (HT-$Ba_3(MnO_4)_2$, $Ba_3(MnO_4)_{2-x}(BO_3)_x$ ($x = 0.031(1)$), $Ba_5(MnO_4)_3Cl$ and $Sr_5(MnO_4)_3OH$). Crystal dimensions were derived from scanning electron microscope (SEM) images recorded on a Jeol JSM-25CF instrument.

Solution state voltammetry

An intensely green saturated (approx. 1 mM) solution of $BaMnO_4$ in fresh Ar-saturated 9 M KOH was prepared and kept under an Ar inert-gas atmosphere. For voltammetric measurements, a 0.5-mm diameter Pt disk working electrode (Micro Glass Instruments, Australia) was used in conjunction with Hg/HgO (9 M KOH) reference and Pt mesh auxiliary electrodes. The cyclic voltammetry software option of an IM5d impedance spectrometer (Zahner, Germany) was used to control the electrochemical cell and collect voltammetric data.

Abrasive stripping voltammetry

The 0.5-mm diameter Pt disk electrode was here effectively polished with the compound to be studied, causing some of the microcrystals to adhere to the electrode surface. Voltammetric measurements were undertaken with the three-electrode setup described above in $Ba(OH)_2$-saturated 9 M KOH electrolyte solutions in order to avoid any dissolution and subsequent disproportionation or oxidation reactions of the studied manganates. Saturation with inert Ar gas and working under this atmosphere ensured that no ambient CO_2 was taken up by the strongly basic electrolyte solution. Cell control and data acquisition methods were identical to those mentioned above.

Table 1 Lattice constants and average Mn-O distances of alkaline earth manganates-(V) and -(VI). Standard deviations are given in parentheses

Compound	Space Group	a [pm]	b [pm]	c [pm]	Mn-O [pm]
$KBaMnO_4$	Pnma	776.81 (4)	582.07 (2)	1027.11 (4)	166.3
LT-$Ba_3(MnO_4)_2$	$R\bar{3}m$	569.95 (2)		2151.59 (5)	170.4
HT-$Ba_3(MnO_4)_2$	$R\bar{3}m$	571.62 (1)		2146.21 (4)	170.9
$Ba_3(MnO_4)_{2-x}(BO_3)_x$	$R\bar{3}m$	571.15 (3)		2145.48 (4)	164.7
$Ba_5(MnO_4)_3OH$	$P6_3/m$	1036.62 (5)		782.58 (2)	171.9
$Ba_5(MnO_4)_3Cl$	$P6_3/m$	1048.0 (4)		776.9 (2)	169.8
$Sr_5(MnO_4)_3OH$	$P6_3/m$	997.10 (3)		746.19 (2)	169.7
$BaMnO_4$	Pnma	910.93 (2)	549.47 (2)	733.12 (2)	167.8

Table 2 Crystallographic systems and approximate crystal dimensions (x length, y width, z height) of alkaline earth manganates-(V) and -(VI)

Compound	Cryst. system	cryst. dim. x/y/z [μm]	comments
$KBaMnO_4$	orthorhombic	1–5/1–5/1–5	intergrown crystals
LT-$Ba_3(MnO_4)_2$	rhomboedric	1/1/1	intergrown crystals
HT-$Ba_3(MnO_4)_2$	rhomboedric	10/10/1	platelets
$Ba_3(MnO_4)_{2-x}(BO_3)_x$	rhomboedric	$10/10/<0.5$	platelets
$Ba_5(MnO_4)_3OH$	hexagonal	1–5/0.5/0.5	intergrown needles
$Ba_5(MnO_4)_3Cl$	hexagonal	–/–/–	agglomerate
$Sr_5(MnO_4)_3OH$	hexagonal	5–10/0.5/0.5	needles
$BaMnO_4$	orthorhombic	1–30/1–30/1–30	intergrown crystals

Results and discussion

Comparing the voltammograms of, e.g., $BaMnO_4$ in solution and solid-state phases (Fig. 2a, b), a redox process centered at $E^\circ = 240$ mV is obvious in solution (Fig. 2a) but not in the solid-state phase (Fig. 2b). Additional voltammetric experiments at varying scan rates confirm that this solution-state reduction process is at least quasi-reversible in the electrochemical sense in the 2–500 mV/s range with a ΔE_p-value of 75–80 mV. Judging by values of peak currents and half-wave potential, the process is assigned to the one-electron reversible reduction of MnO_4^{2-} to MnO_4^{3-}. Further reduction steps are detected upon scanning to more negative potentials, and they most probably include thermodynamically favored MnO_2 film formation from about 100 mV onwards. Subsequent MnO_2 reduction to yield MnOOH and finally $Mn(OH)_2$ at −200 and −350 mV, respectively, are processes which are well documented in the literature (see, e.g., [17]), and leave the electrode surface covered with corresponding solids.

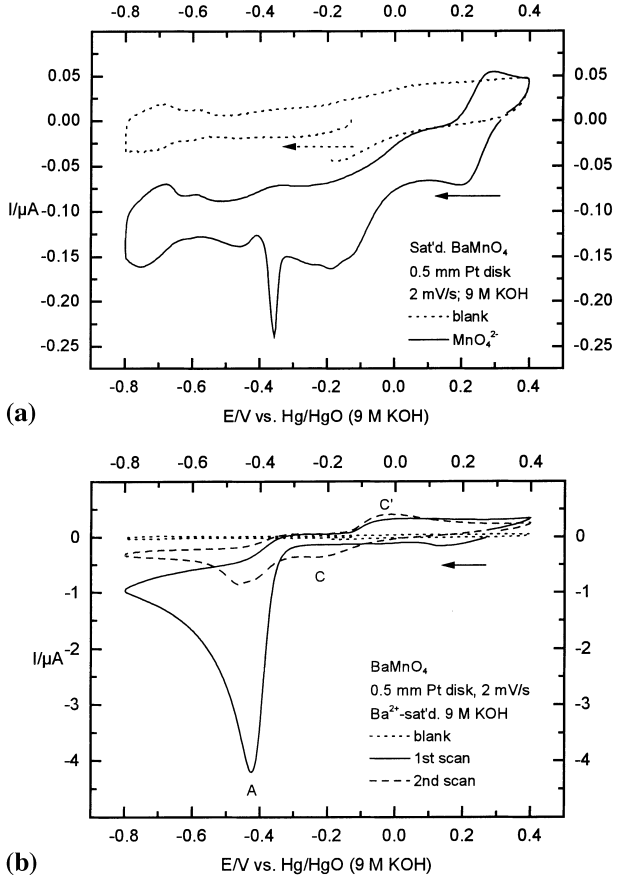

Fig. 2 a Solution state cyclic voltammetry of approx. 1 mM $BaMnO_4$ in 9 M KOH at a 0.5-mm diameter Pt disk electrode. Scan rate: 2 mV/s. **b** Cyclic abrasive stripping voltammetry of $BaMnO_4$ when mechanically attached to a 0.5-mm diameter Pt disk electrode in Ba^{2+}-saturated 9 M KOH. Scan rate: 2 mV/s. The same background voltammogram of the 0.5-mm diameter Pt disk electrode in 9 M KOH is shown as *dotted line* in Fig. 2a and b

When scanning towards more positive potentials, from about 100 mV these layers are removed by sluggishly responding re-oxidation processes, and MnO_4^{3-} oxidation becomes the dominant process. Upon adding $Ba(OH)_2$ to the electrolyte solution, green $BaMnO_4$ precipitates, and the voltammetric response fades accordingly, eventually resembling that of the blank KOH solution.

The solid-state voltammogram of $BaMnO_4$ (Fig. 2b) shows substantially larger peak currents for all detected processes than those of the solution state. In particular, there is no significant reductive response in the potential region 250 to −300 mV, which leads us to conclude that the observed electrochemical reduction in the solid-state phase does represent a multiple-electron reduction process. The responses in the case of dissolved MnO_4^{2-}, which have been attributed to conversions of products involving solid-state phases, occur at significantly different peak potentials, peak currents and with different shapes than those observed when investigating the pure solid, $BaMnO_4$.

All manganates studied in the solid-state phase show one irreversible reduction signal between −380 and −470 mV relative to an Hg/HgO (9 M KOH) reference electrode, labeled A in Figs. 2b–5 and 7–9, and A1 and A2 in Fig. 6. All relevant voltammetric data is contained in Table 3. Previously published work on the electrochemistry of non-conducting solids when attached to the surface of an electrode [6] teaches that peak potential, peak current and peak shape all depend on the amount as well as the particle size parameters of the studied solid. However, we experience rather uniform behaviour in terms of peak potential E_p and peak shape in the case of the manganates investigated in this work. Accordingly, while peak currents may vary by up to 30%, E_p-values obey the relationship $E_p =$ const. ± 5 mV for each compound when averaged over independent voltammetric experiments on different samples. The general stability of solid manganates-(V) and -(VI) towards reduction is remarkable, especially when compared to,

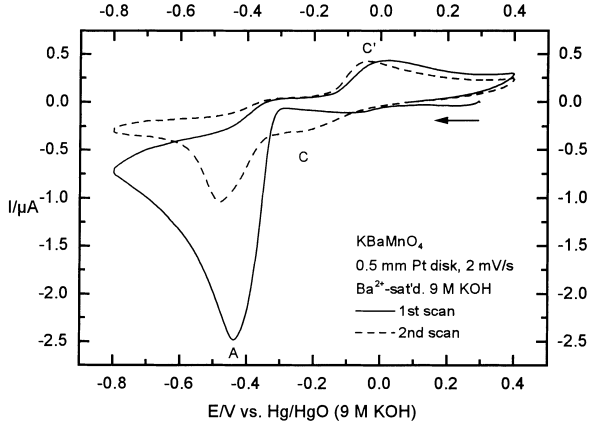

Fig. 3 Cyclic abrasive stripping voltammetry of $KBaMnO_4$ when mechanically attached to a 0.5-mm diameter Pt disk electrode in Ba^{2+}-saturated 9 M KOH. Scan rate: 2 mV/s

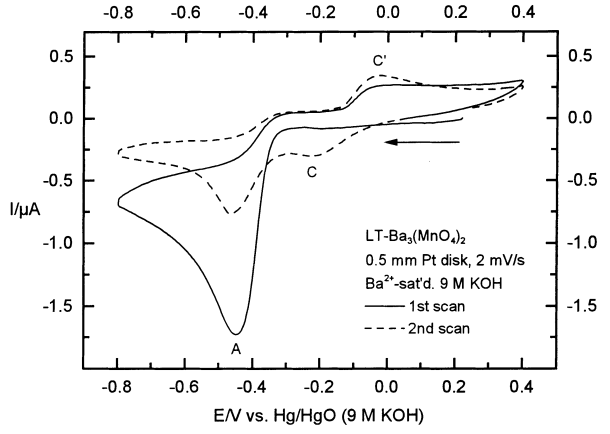

Fig. 4 Cyclic abrasive stripping voltammetry of LT-$Ba_3(MnO_4)_2$ when mechanically attached to a 0.5-mm diameter Pt disk electrode in Ba^{2+}-saturated 9 M KOH. Scan rate: 2 mV/s

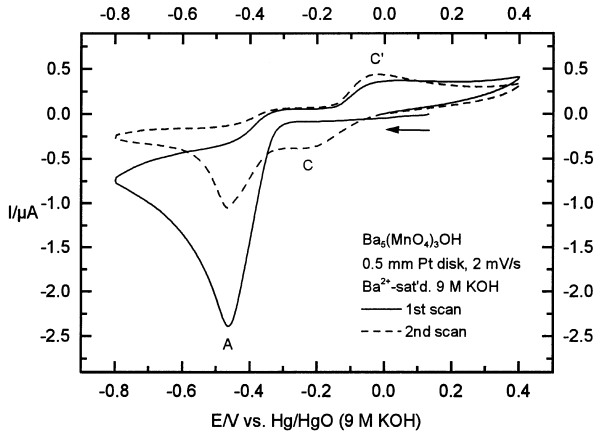

Fig. 7 Cyclic abrasive stripping voltammetry of $Ba_5(MnO_4)_3OH$ when mechanically attached to a 0.5-mm diameter Pt disk electrode in Ba^{2+}-saturated 9 M KOH. Scan rate: 2 mV/s

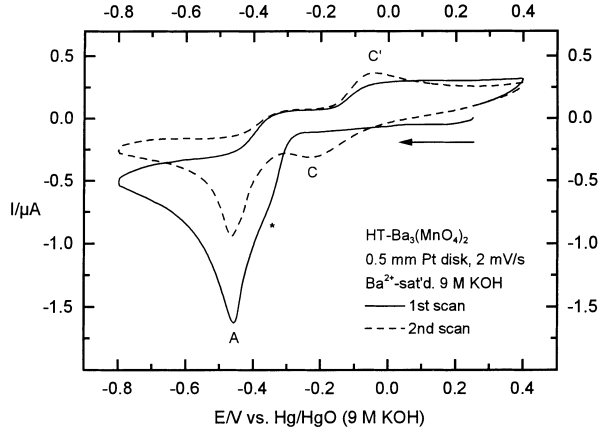

Fig. 5 Cyclic abrasive stripping voltammetry of HT-$Ba_3(MnO_4)_2$ when mechanically attached to a 0.5-mm diameter Pt disk electrode in Ba^{2+}-saturated 9 M KOH. Scan rate: 2 mV/s

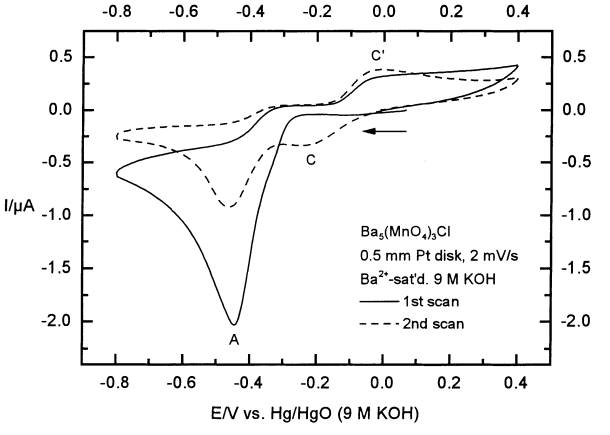

Fig. 8 Cyclic abrasive stripping voltammetry of $Ba_5(MnO_4)_3Cl$ when mechanically attached to a 0.5-mm diameter Pt disk electrode in Ba^{2+}-saturated 9 M KOH. Scan rate: 2 mV/s

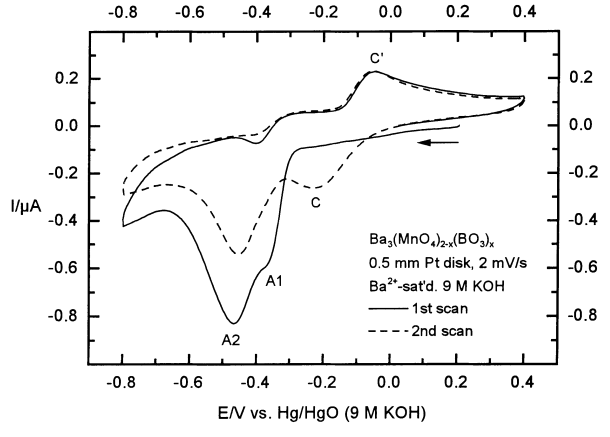

Fig. 6 Cyclic abrasive stripping voltammetry of $Ba_3(MnO_4)_{2-x}(BO_3)_x$ ($x = 0.031(1)$) when mechanically attached to a 0.5-mm diameter Pt disk electrode in Ba^{2+}-saturated 9 M KOH. Scan rate: 2 mV/s

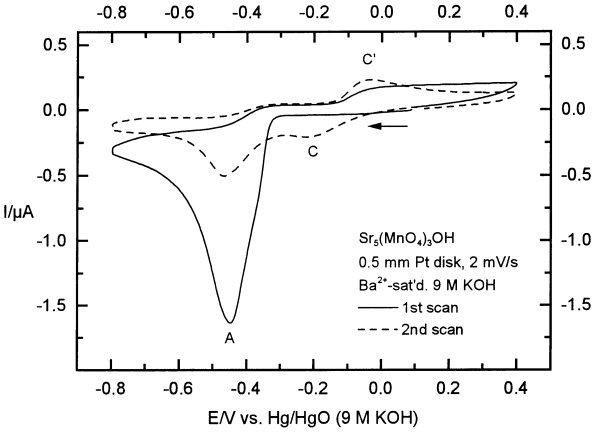

Fig. 9 Cyclic abrasive stripping voltammetry of $Sr_5(MnO_4)_3OH$ when mechanically attached to a 0.5-mm diameter Pt disk electrode in Ba^{2+}-saturated 9 M KOH. Scan rate: 2 mV/s

Table 3 Peak potentials E_p and peak currents I_p of processes A, C′ and C of voltammograms of surface-attached alkaline earth manganates-(V) and -(VI) shown in Figures 2b to 9. Values for processes C′ and C are taken from corresponding second voltammetric scans.

Compound	E_p(A) [mV]	I_p(A) [μA]	E_p(C′) [mV]	I_p(C′) [μA]	E_p(C) [mV]	I_p(C) [μA]
$KBaMnO_4$	−437	−2.49	−37	0.43	−241	−0.30
LT-$Ba_3(MnO_4)_2$	−449	−1.73	−25	0.34	−228	−0.30
HT-$Ba_3(MnO_4)_2$	−456	−1.63	−40	0.36	−232	−0.31
$Ba_3(MnO_4)_{2-x}(BO_3)_x$	−382[a]	−0.60[a]	−47	0.23	−233	−0.26
	−465[b]	−0.83[b]				
$Ba_5(MnO_4)_3OH$	−464	−2.93	−16	0.44	−256	−0.38
$Ba_5(MnO_4)_3Cl$	−445	−2.03	−7	0.38	−245	−0.34
$Sr_5(MnO_4)_3OH$	−449	−1.64	−34	0.23	−232	−0.21
$BaMnO_4$	−424	−4.21	−12	0.41	−236	−0.36

[a] Data for shoulder labeled "A1" in Fig. 6
[b] Data for peak labeled "A2" in Fig. 6

e.g., the solution behavior of the MnO_4^{2-} ion in 9 M KOH, as discussed before, or the solid-state voltammetric response of γ- or δ-MnO_2 [9, 17].

Considering the observed reduction potential range of −370 to −470 mV, reduction signals of all investigated manganates-(V) and -(VI) (Figs. 2b–9) are attributed to the overall three- or four-electron solid-state electrochemical reduction of formally penta- or hexavalent manganese to yield Mn-(II), respectively [17].

The observed reduction behaviour of solid manganates is thus believed to be a multiple-electron process. Single steps cannot be fully resolved, and it therefore remains unclear whether either one of the three or four one-electron reduction steps for manganates-(V) or -(VI), respectively, is generally reversible. However, the overall observed process is certainly irreversible, and a new product with a corresponding redox process C/C′ centered at about −140 mV is generated (Figs. 2b–9).

Peak currents are generally defined by the total number of electrons transferred through faradaic processes, charging currents neglected. The same electrode was used for all measurements, and, as judged by observation with the naked eye, always a similar coverage of the electrode surface with each compound was achieved. Comparable peak currents between −1.5 and −2.5 μA are observed for almost all manganates-(V) (see Figs. 3–5 and 7–9). $Ba_3(MnO_4)_{2-x}(BO_3)_x$ which crystallizes in fairly large platelets, reproducibly showed smaller peak currents (Fig. 6). This is tentatively attributed to the relatively small amount of compound being attached to the electrode surface, assuming that single platelets lie essentially flat on the surface of the electrode. This may be compared to, e.g., LT-$Ba_3(MnO_4)_2$ (Fig. 4), which crystallizes as strongly intergrown platelets and therefore results in a larger surface area when being attached to an electrode surface. LT- and HT-$Ba_3(MnO_4)_2$ are characterized by low and high crystallinity, respectively. However, the peak currents appear to be related to the shortest crystal dimension, which is about 1 μm for each sample, as judged by the measured approximately equal peak current values (Figs. 4, 5 and Table 2). $BaMnO_4$ (Fig. 2b) shows a comparatively larger peak current, and this is related to the transfer of one more electron per overall reduction process of this manganate-(VI). As discussed above, another current-enhancing effect is seen in the finely grained and strongly intergrown crystal appearance of $BaMnO_4$ (see Table 2).

As for peak positions, it must be taken into account that the overlap of three or four one-electron steps, respectively, leads to the observed peak positions. Any rate-determining dissolution process, which could be anticipated to a limited extent for intermediate manganese-(III) species [18], would be expected to shift peak potentials to more negative values. However, the used barium-saturated electrolyte solutions are known to suppress dissolution of manganates-(III) on the experimental time scale [18] at the same applied voltammetric scan rate of 2 mV/s. We therefore believe that dissolved products and hence accompanying kinetic effects on the voltammetric response of the studied manganates-(V) and -(VI) are limited.

With samples of high crystallinity, more or less pronounced peak splitting along with more symmetric peak tips are observed. Hence, the peak shape appears to be somehow connected to the crystallinity of a particular manganate. In the case of HT-$Ba_3(MnO_4)_2$, an additional shoulder appears at about −350 mV labeled * in Fig. 5, which could be due to some splitting of the multiple-electron reduction process confined to the solid-state phase assumed above. In the case of $Ba_3(MnO_4)_{2-x}$ $(BO_3)_x$ (Fig. 6), the reduction signal is more obviously split into two signals of approximate current ratio 2:1, which supports splitting of the (in this case) overall three-electron reduction process into a two- and a one-electron reduction process, A1 and A2, respectively. A similar effect, although not as pronounced, is obvious for the reduction of both $Ba_5(MnO_4)_3Cl$ (Fig. 8) and $Sr_5(MnO_4)_3OH$ (Fig. 9). An explanation for these peak splittings can, be given on the grounds of either kinetics or thermodynamics. Different crystallographic sites can be expected to exhibit different reaction kinetics in general. Alternatively, one may take into account that formation of products is thermodynamically controlled, and some resolution of the individual one-electron reduction steps becomes

visible. For example, in the rather extreme case of $Ba_3(MnO_4)_{2-x}$ $(BO_3)_x$ (Fig. 6), the main kinetic contribution would be expected to be related to reduction perpendicular to the relatively large platelets (cf. Table 2), and this would result in one voltammetric signal for the overall reduction process when the influence of dissolution kinetics can be neglected as outlined above. We therefore think that the actually observed peak splitting at least in this case reflects thermodynamic properties of the manganate. Furthermore, all $Ba_3(MnO_4)_{2-x}(BO_3)_x$ seems to be exhaustively consumed during the first voltammetric scan as evidenced by the missing peak splitting during the second scan. The consequence of this is that the observed reduction process in the −450 mV region during the second scan is characteristic of the product defined by the redox process C/C′.

As already mentioned twice, the chemically reversible process labeled C/C′ in Figs. 2b–9 appears to be related to products of the irreversible reduction process A. Interestingly, this process C/C′ appears to be a common feature in terms of both peak potential and peak current of the studied manganates-(V) and -(VI) and is a subject of current studies. The (so far) assumed [5–7] yet unspecified charge-balancing incorporation of counter-ions from the surrounding electrolyte solution upon reduction is expected to play a role in that respect. Alternatively, dissolution of reduction products may occur in order to reach a charge balance upon reduction. For example, $BaMnO_4$, $KBaMnO_4$, LT-$Ba_3(MnO_4)_2$, $Ba_5(MnO_4)_3OH$, $Ba_5(MnO_4)_3Cl$ and $Sr_5(MnO_4)_3OH$ show a small loss when roughly comparing the total charges consumed during four- or three-electron reduction (process A) with those of the subsequent one-electron oxidation (process C′) (see Figs. 2b–4 and 7–9). However, the secondary redox process C/C′ is observed regardless of this loss of compound (see Figs. 2b–9). Moreover, the lower the apparent loss of reduction products, the higher is the relative amount of generated product, i.e., the larger is the observed relative response of process C/C′. This is clearly observed with either HT-$Ba_3(MnO_4)_2$ or $Ba_3(MnO_4)_{2-x}(BO_3)_x$ (see Figs. 5 and 6). Hence, we can safely assume that any loss of direct reduction products by dissolution merely reduces the amount of the product characterized by the redox process C/C′. Consequently, this product is strongly believed to be generated through a solid-state transformation. Whether the reduction mechanism obeys the rules of either nucleation/growth [7, 8], dissolution/precipitation [8], or the recently published miscibility gap concept [19] remains at present open to discussion.

The average interatomic Mn-O distances in the MnO_4^{x-} groups in these compounds are correlated with the corresponding first observed electrochemical reduction potentials in Fig. 10.

The extent of reduction is clearly reflected by the Mn-O bond lengths, and thus the formal oxidation states, of tetrahedrally coordinated Mn. The high-temperature

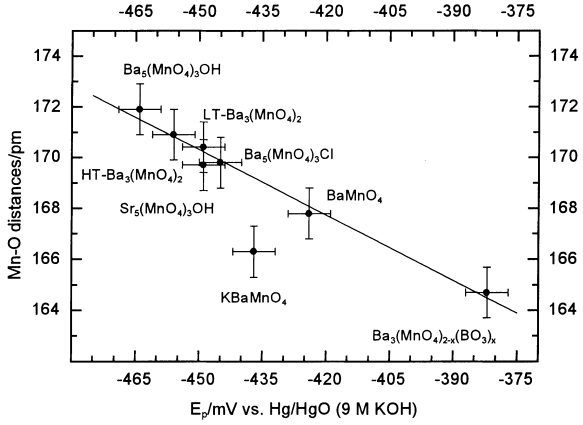

Fig. 10 Correlation between average interatomic MnO distances and electrochemical reduction peak potentials of manganates-(V) and -(VI) as indicated

phase of $Ba_3(MnO_4)_2$ is slightly more stable towards reduction than the low-temperature phase, as would be expected from the larger crystal size and improved crystallinity, corresponding to a reduced amount of lattice disorder and thus smaller full-width-at-half-maximum (FWHM) values in the measured diffractograms.

As far as dissolution effects are concerned, $BaMnO_4$, as the most soluble manganate in the presented series, shows no more extraordinary behavior than that of either $Ba_5(MnO_4)_3Cl$ or $Ba_3(MnO_4)_{2-x}(BO_3)_x$ (cf. Fig. 10), both of which were found to be highly insoluble in the used electrolyte solution. This result in our view supports the assumption that rate-limiting dissolution effects are negligible with respect to their influence on peak positions.

$KBaMnO_4$ appears to be more stable towards reduction than the other manganates-(V) and -(VI). We see an explanation in the differing ratios of numbers of counter-ions per $(MnO_4)^{x-}$ entity. In $KBaMnO_4$, two cations (K^+ and Ba^{2+}) compensate for one MnO_4^{3-} entity, while in, e.g., $Ba_3(MnO_4)_2$, three cations (Ba^{2+}) make up the charge balance for two MnO_4^{3-} units. Consequently, upon reduction, the introduction of charge-balancing counter-ions into the lattice of $KBaMnO_4$ would be suppressed relative to $Ba_3(MnO_4)_2$.

Conclusions

Reduction peak potentials of a number of barium and strontium manganates-(V) and -(VI) in the solid state were determined using abrasive stripping voltammetry. A linear correlation was found between voltammetric data and the corresponding average Mn-O distances calculated from X-ray powder diffractometric data by Rietveld refinement analyses. On the grounds of additional voltammetric experiments on dissolved manga-

nate-(VI), we believe that truly solid-state electrochemical processes are observed when solid strontium and barium manganates-(V) and -(VI) are being attached to the surface of an electrode and subjected to a voltammetric experiment in barium-saturated 9 M KOH. Under the applied conditions, abrasive stripping voltammetry is currently thought to mainly reflect the thermodynamic properties of solid microcrystalline manganates-(V) and -(VI). However, strictly speaking, future studies regarding the kinetics of such manganates are required in order to find out whether the assumed negligibility of any dissolution of intermediates holds, and, consequently, whether the found dependence of AbrSV peak potentials on corresponding Mn-O distances allows this conclusion to be drawn. Whether or not the corresponding mechanism obeys the rules of either nucleation and growth, dissolution/precipitation, or the recently published miscibility gap concept remains open to discussion.

Acknowledgements This study has been funded by the Austrian Fonds zur Förderung der wissenschaftlichen Forschung' as projects P11099-ÖCH and M00383-CHE. Additional support through the 'Spezialforschungsbereich Elektroaktive Stoffe' is acknowledged.

References

1. Scholz F, Nitschke L, Henrion G (1989) Naturwissenschaften 76: 71
2. Scholz F, Nitschke L, Henrion G, Damaschun F (1989) Fresenius Z Anal Chem 335: 189
3. Scholz F, Lange B (1992) Trends Anal Chem 11: 359
4. Scholz F, Lange B (1994) Chem Soc Rev 23: 341
5. Bond AM, Marken F (1994) J Electroanal Chem 372: 125
6. Bond AM, Colton R, Marken F, Walter JN (1994) Organometallics 13: 5122
7. Bond AM, Fletcher S, Marken F, Shaw SJ, Symons PG (1996) J Chem Soc Faraday Trans 92: 3925
8. Bond AM, Fiedler DA (1997) J Electrochem Soc 144: 1566
9. Fiedler DA, Besenhard JO, Fooken MH (1997) J Power Sources 69: 157
10. Rosenstiehl J (1864) J Pharm 46: 344
11. Lux H (1946) Z Naturforsch 1: 281
12. Scholder R, Klemm W (1954) Angew Chem 66: 461
13. Scholder R (1958) Angew Chem 70: 583
14. Brixner LH, Weiher JF (1968) Inorg Chem 7: 1474
15. Albering JH, Besenhard JO (1997) Z Kristallogr, Suppl 12: 46
16. Izumi F (1985) J Crystallogr Soc Jpn 27: 23
17. McBreen J (1975) Electrochim Acta 20: 221
18. Fiedler DA (1998) J Solid State Electrochem 2: 315–320
19. Scholz F, Lovrić M, Stojek Z (1997) J Solid State Electrochem 1: 134